Green Chemistry

ROYAL SOCIETY OF CHEMISTRY

PAPER

View Article Online
View Journal | View Issue

Cite this: *Green Chem.*, 2023, **25**, 9959

Design principles for $LiFePO_4$ electrodes with improved recyclability†

Lechen Yang, Dominika Gastol and Emma Kendrick *

Received 17th October 2023,
Accepted 2nd November 2023

DOI: 10.1039/d3gc03970f

rsc.li/greenchem

To improve sustainability of lithium-ion battery electrodes there is a need to design in recycling at the manufacturing stage. In this work, a method to improve $LiFePO_4$ recovery rates through binder and electrode microstructure design is presented. Electrodes are produced by tape cast and direct ink writing methods with biopolymer, aqueous binder systems: carboxy-methyl cellulose with styrene butene rubber, or sodium alginate, with and without a secondary solvent rheology modifier, octanol. The recovery rate of the active material is measured after a short low power ultrasound delamination process, performed in water. Electrodes which exhibit good wettability, as observed through low contact angles, and low tortuosity, delaminate faster with higher recovery rates. Improvements from 2% to 60% black mass recovery is observed with CMC-SBR electrodes with the addition of octanol in the electrode inks, and from 79% to 86% in direct-ink printed compared to tape cast electrodes when using alginate binders. These results highlight the importance of electrode design in the circular manufacturing and recycling of LIBs and lay the groundwork for future research into new design principles for printed electrodes.

Introduction

Lithium-ion batteries (LIBs) have emerged as a vital technology for enabling a sustainable future, particularly in achieving Net Zero targets through electrification of transportation and the power grid. As the demand for energy storage continues to rise, the recycling of LIBs becomes crucial for resource conservation and the circular economy, with 70% recycling required by 2030.[1] To address this, it is imperative to develop sustainable and efficient recycling processes that adhere to green principles of sustainability, engineering, and chemistry.[2] The recycling of LIBs typically begins with the collection and sorting of batteries. Sorting batteries based on their chemistries plays a pivotal role in creating purer material streams and facilitating more effective recycling. The cells are typically shredded, and the waste then size separated. Physical separation methods, such as sieving and magnetic separation, can be employed as pre-treatment steps to segregate various components.[3] These separation techniques enable the extraction of valuable components, such as coated aluminium and coated copper, while pre-separating graphite from transition metals, thus generating purer material streams for further processing and minimizing dissolution.[4] Further separation and purification can be achieved through hydrometallurgical methods, such as leaching and solvent extraction.[5] One of the key challenges in LIB recycling is the separation of different materials in shredded battery waste to prevent cross-contamination. This necessitates the exploration of innovative techniques and processes for effective material separation. Disassembly techniques can enhance the separation of different components, leading to higher-purity material streams for downstream processing. The purity and quality of the recycling feedstock directly impact the value and sustainability of the recycling process, underscoring the importance of optimizing material recovery.[6,7] To prevent waste, the recovery rates of all components within the cell require maximising. Current collectors and active material components can be recovered through 'design for disassembly' methods. This requires careful choices for solvents and binders used in the electrode fabrication processes. Renewable and biodegradable feedstocks, can be used with safer solvents and auxiliaries, such as water, for manufacture of electrodes, substituting for the harmful *N*-methyl pyrrolidone (NMP) solvent and polyvinylidene fluoride (PVDF) binder which has been traditionally used.[8] PVDF is classed as a per and polyfluoroalkyl substance (PFAS) which has serious implications due to the future widespread ban on their uses and production in Europe.[9] Fluorinated polymers can be made through emulsion-based reactions which can lead to PFAS contamination and has been documented to be harmful to health and the environment.[10] PVDF is also known to be extremely stable and highly resistant to breakdown in an ambient environment, posing challenges in recycling and sustainability.[11] Microplastics and thermal degradation of these

Energy Materials Group, School of Metallurgy and Materials, The University of Birmingham, Edgbaston, Birmingham, B15 2SE, UK. E-mail: E.kendrick@bham.ac.uk

† Electronic supplementary information (ESI) available. See DOI: https://doi.org/10.1039/d3gc03970f

materials may release further contamination and routes for recycling fluorinated polymers need to be seriously investigated.[12] Water-soluble green bio-polymer binders have gained significant interest due to their processability in manufacturing and their ease of removal using water, allowing for the liberation of active materials from the current collector and the binders during recovery.[13–15] Alternative binders, including carboxyl methyl cellulose (CMC)[16,17] and other bio-based options such as alginate and xanthan gum,[18–22] offer sustainable alternatives with reduced environmental impact and improved recyclability.

The electrode manufacturing process of electrodes should also be carefully considered, both in terms of waste production, ease of processability, flexibility, but also its effect upon the recyclability. Among slurry casting techniques, the draw-down technique is the most widely used method in research, whereas slot-die or comma bar is used in industry.[23–26] Studies have suggested that very little real-time control of the electrode deposition is possible using these techniques, therefore, alternative electrode manufacturing routes, specifically additive manufacturing techniques are now being explored in electrode manufacturing.[27] Gastol *et al.* have illustrated the feasibility of employing digital syringe deposition printing methods for designing increased coat weight graphite electrodes, which exhibited longer cycle life on account of the optimised ion transport network.[28] Yet admittedly, further optimisation on inks with battery electrodes is required.[29] Studies on patterned electrodes have focused on enhanced electrochemical performances such as higher areal capacity or capacity retention,[29–31] however electrode design can also be linked to recovery rates in recycling processes.[6,32]

This work aims to provide a more holistic approach to electrode design for greater sustainability, considering both manufacturing and recycling processes together. A novel electrode design is proposed and demonstrated for $LiFePO_4$ (LFP).[33–35] This design uses a 3D printing manufacturing process which produces less waste during the production of electrodes compared to current industrial processes, and the 3D electrode structure maximises the efficiency for material recovery when recycled using a low energy separation process. Renewable binder feedstocks with a safe and benign solvent, water, are used, these impacts both the manufacturing and recycling processes of $LiFePO_4$ electrodes. The ink requires modification and the rheological properties optimised, so that the structure of the print is retained, this is performed with a biodegradable secondary solvent. The binders can also biodegrade thus reducing contamination and waste upon recycling, and they substitute for PVDF which can only dissolve in limited solvents such as NMP, providing a more sustainable alternative binder-solvent system. The electrode designs provide good electrochemical performance whilst also allow for efficiency optimisation of the recycling process for production of high purity and quality recycling feedstock. Thus, this holistic approach can foster a more sustainable and circular economy for lithium-ion battery electrodes.

Materials and methods

Electrode preparation

The cathode LFP (Gelon) with a particle size ~0.5 μm was mixed into a slurry using a Thinky ARE 250 centrifugal mixer (Thinky, USA) in an 86.50 : 7 : 6 ratio of active, carbon and binder. 1.5% CMC (Bondwell BVH8, Ashland) with 3% SBR (BM-451B Zeon), or 3% sodium alginate (Alfa Aesar). NaAlg binder solution was used, into which 0.5% short carbon nanotubes (Nanocyl, Belgium) and conductive additive (Timcal C65, Imerys) were added before the LFP. Half of the binder material (either CMC or alginate) was first added together with the dispersed CNT using IKA applicator (T25 digital Ultra Turrax) at 5000 rpm for 10 minutes. The conductive carbon and water were then added into the slurry at 7000 rpm for 10 minutes, followed by 500 rpm for 1 minute, 2000 rpm for 10 minutes and 2200 rpm for 3 minutes (degassing program) using the Thinky Mixer. LFP was then added together with the other half of the binder material, which was mixed using IKA applicator at 7000 rpm for 10 minutes, followed by 500 rpm for 1 minute, 2000 rpm for 10 minutes and 2200 rpm for 3 minutes (degassing program) using the Thinky Mixer again. 1-Octanol (Alfa Aesar) was added to the mix, at 1300 rpm for 5 minutes, before any SBR was added at 500 rpm for 10 minutes. **Rheology:** the rheological behaviour of the LFP-based slurries was investigated with the use of a rotational Rheometer (Malvern) Kinexus, bottom plate: PLS61 S4769 SS, top plate: OP4/40 SR5463 SS by applying table of shear rates 0.1–100 s^{-1} and strain amplitude sweep, starting shear strain from 0.01% to 100% at frequency of 1 Hz with 10 sample per decade. All conducted measurements of the inks were performed at 25 °C. **Draw-down electrodes:** the as prepared slurries were coated onto the aluminium foil using a draw-down coater (K Paint Applicator, RK Printcoat Instruments, UK) *via* a doctor blade with ~250 μm blade gap. The prepared coatings were dried on a hot plate at 50 °C and then transferred to the vacuum oven and dried at 120 °C. Calendaring was performed at ambient temperature to around 40% porosity with the use of MTI calendar. **Printed electrodes:** the ink preparation method used in printing was the same as draw-down coatings, where both CMC/SBR and Na–alginate have been applied to test their feasibility for 3D printed electrodes. Addition of 0.5 wt% 1-octanol was tested to examine its ability for modifying the rheological behaviours of the ink to enable precise digital deposition. Here, the GV Series Automated Dispensing System (Nordson) was applied. The DispenseMotion™ controller, the Gantry Robots, and the dispensing system components comprised the digital printing setup. *Via* a pre-programmed computer software, the ink was designed to fill a rectangular area of 6.5 × 4.5 cm^2 on a carbon-coated Al current collector following an S path (Fig. S1†) Through the movement of the Gantry Robot, ink was deposited in a non-contact manner into the current collector by a 330 μm diameter stainless-steel needle tip attached to a dispensing nozzle. The printing process was operated at a running speed of 100 mm s^{-1}, line width 0.70 mm under a pressure of 40 psi. The carbon-coated Al

current collectors (CAL) were used for printed electrodes to improve its adhesion.

Electrochemistry tests

The coat weight of the electrodes was adjusted to achieve areal capacity of approx. 1 mA h cm^{-2} for a specific capacity of 160 mA h g^{-1}. Dried coatings were processed in a dry room with a dew point of −45 °C. 2032 coin cells were constructed with positive electrode discs 14.8 mm in diameter (cathode half-cell), tri-layer 2025 separator (Celgard) and lithium metal disc acting as a counter electrodes (15.0 mm, 70 μm thick) filled with 70 μm of 1 mol L^{-1} 1.0 M $LiPF_6$ in EC/EMC (ethylene carbonate/ethyl methyl carbonate) 3/7 (v/v) + 2 wt%. VC (vinylene carbonate) electrolyte and sealed with a hydraulic crimper (MSK-110, MTI Corporation, USA), as demonstrated in Fig. S2.† The coatings were tested electrochemically in the coin cells half-cells. Electrochemical testing was performed on a Bio-Logic BCS 805 series cycler. Initial capacities and formation were obtained by applying the following protocol: 10 mA g^{-1} for the anode half cell: lithiation 1.0 V *vs*. Li/Li+ and delithiation to 2.5 V *vs.* Li/Li+, whereas for the cathode half-cells: charge to 3.95 V *vs*. Li/Li+ and discharge to 2.8 V *vs*. Li/Li+. For both types of cells, the same steps were repeated twice. The same test was repeated for three times in total for each type of the samples, where an average 1st cycle charge/discharge capacity can be obtained with standard deviation corresponding to the error bars.

Additionally, current density testing was performed by applying three cycles between rates of 0.25 C and 7.5 C, *i.e.* 40 mA g^{-1}, 80 mA g^{-1}, 160 mA g^{-1}, 320 mA g^{-1}, 500 mA g^{-1}, 800 mA g^{-1}, 1200 mA g^{-1} and 40 mA g^{-1}. Followed by cycling by setting 80 mA g^{-1} (C/2 rate) at the charge and 160 mA g^{-1} (C rate) for the discharge cycles, respectively, for total of 100 cycles for the test. The cycling tests were repeated for 3 times in total for each type of the cell, and the best performing cell among the repeats in this case will be chosen.

Electrode delamination (separation) and characterisation

The as-prepared samples were first cut into 65 mm × 45 mm pieces by scissors, in order to standardize the tests. Each sample then placed in a beaker inside an ultrasonic bath (MEB Total Limited). A varying active material to water ratio of 1 : 20, 1 : 50, and 1 : 100 was applied in this case for all types of the electrodes involved in this study. The ultrasonic power applied was 50 W under ambient temperatures for 1–10 minutes. The reclaimed powder was washed with distilled water to remove the residues and centrifuged at 4000 rpm for 20 minutes to recover the materials. Two further repeats were performed for each type of electrode, using the same active material to water ratio, to assess reproducibility. An average separation efficiency was calculated, with the standard deviations corresponding to the error bars. Any remaining active materials attached to the current collectors after washing were regarded as unseparated. The sediments were further dried and collected (black mass). The separation rate of active materials from the current collectors[36] was calculated using eqn (1), where m_0 is the weight of the current collector of the same size, m_1 is the weight of electrode before separation and m_2 is the weight of electrode after separation (assuming the weight of the current collector stays constant).

$$\text{Peel-off efficiency} = \frac{m_1 - m_2}{m_1 - m_0} \times 100\%. \quad (1)$$

Contact angles

Contact angles were measured by a Contact Angle Goniometer (Ossila Contact Angle, UK) to investigate differences in wettability. Here, the samples were attached to the glass slide, and a droplet of 10 μL distilled water was dripped onto the sample surface in 5 different spots. The obtained contact angles were then averaged to achieve the final result, along with the standard deviation representing the error bars.

The surface morphology of the coating materials before and after separation process was characterized by **Scanning electron microscopy** (SEM, Hitachi 3030+ Desktop) and the element compositions were detected by Energy Dispersive X-ray Spectroscopy (EDS). Particularly, representative coatings were cross-sectioned and observed under SEM to identify the existence of microchannels. The cross-sectional micrographs were analyzed using the TauFactor add-in,[37] in Matlab to calculate tortuosity of the coatings, where the tortuosity of the coating can be automatically calculated with the input of a cross-sectional SEM image.

Evaluation

In the end, the results were collected and put into a self-designed assessment matrix **ERADE** (Electrode Recyclability and Design Evaluation), as shown in Table S1.† Several criteria, material range, ink readiness, design versatility, economic viability, electrochemical performance, recyclability, are considered and a score assessed for each type of coating produced by different methods:

- Starting from an initial score of 0, scores of 0–5 are given for both draw-down and printed electrodes in terms of each criterion on different aspects of electrode manufacturing, which are then summed.
- A higher score represents an electrode format that is more focussed on green chemistry principles.

Results and discussion

The two binders CMC/SBR or NaAlg, were investigated for suitability with $LiFePO_4$ using a standard draw-down method to produce electrodes. In order to modify the inks for suitability for direct ink writing, 1-octanol was added to decrease the flowability of the ink as performed previously,[28] this secondary solvent addition produced inks which were readily extruded, reduced slumping and produced patterned electrodes. Rheological properties of the inks are presented in Fig. 1(a) and (b), respectively. Viscosity *vs.* shear rate in Fig. 1(a) indicates shear thinning behaviour of all tested inks. NaAlg based

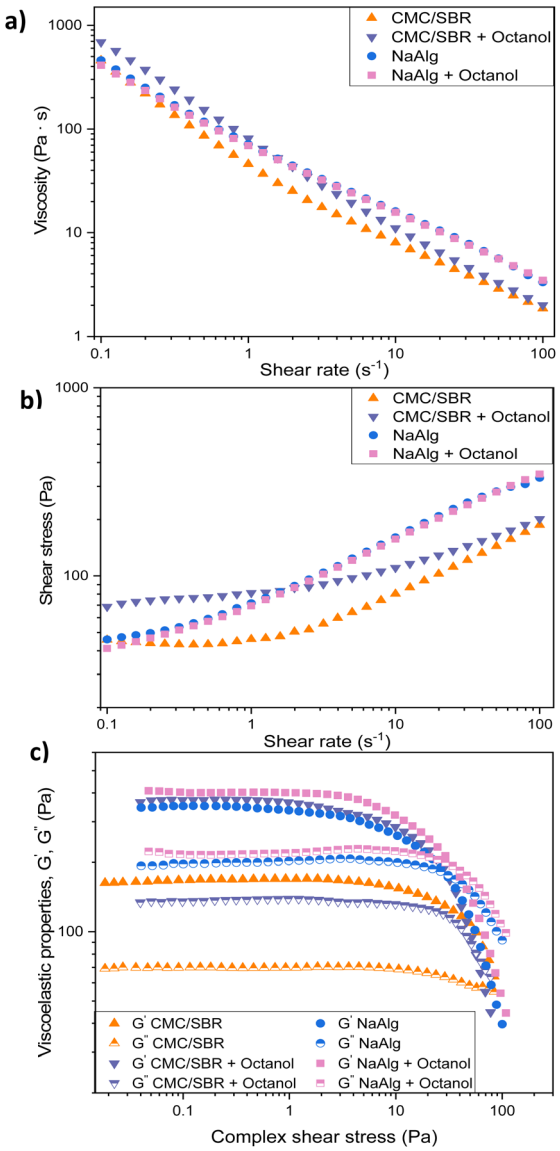

Fig. 1 Rheological properties of the LFP prepared inks, viscosity (a), shear stress (b) *vs.* shear rate and oscillatory rheology (c), respectively.

inks without and with the addition of 1-octanol, exhibited more Newtonian behaviour from approximately 2 s^{-1}. This can indicate that polymer chains of alginate macromolecules are oriented along the extrusion flow direction.[38] It can be also observed that CMC/SBR + octanol ink demonstrates higher viscosity than the same slurry but without the addition of the secondary fluid. This ink exhibits an ideal shear thinning behaviour at the tested shear rates. The oscillatory rheology, presented in Fig. 1(c), demonstrates that octanol addition to the slurries increase both G' and G'' for both binder system tested. However, ink prepared with CMC/SBR + octanol exhibits more significant increase in comparison with alginate-based ink. All the investigated slurries show G' and G'' crossover that allows to determine the yield stress, that indicates the force required to break up the structure and start the material to flow. The σ_o values were obtained from the intersection of the low shear stress (in the linear range of viscoelasticity) and those at higher shear stress values (in the nonlinear range of viscoelasticity), derived from G', presented in the Fig. 2c. It can be noted that the σ_o increases for the NaAlg + octanol in comparison with slurry composed of NaAlg only and decreases when 1-octanol is added when CMC/SBR binder is applied. The highest value of σ_o (25.6 Pa) was observed for the NaAlg + octanol ink that would indicate the strongest structure formed between the LFP, used binder and secondary fluid.

Fig. 2(a)–(c) shows examples of the produced printed electrodes during this study. The printing line spacing varied in different electrodes: ~0.32 mm spacing in Fig. 2(a), ~0.64 mm spacing in Fig. 2(b), and ~0.64 mm spacing in Fig. 2(c). However, the coat weight (~1 mA h cm^{-2}) was kept the same for electrodes to enable direct comparison. Meanwhile, Fig. 3(a)–(d) show the cross-sectional SEM micrographs of both coating produced by the draw-down and the printing method. As can be seen, channels were formed in the printed electrodes.

Fig. 4 shows the first cycle electrochemical performances of all the electrodes. As can be seen, the formation capacities, first cycle columbic efficiency (CE%) and the rate capability for all the electrodes were very similar, as expected with the areal coat-weights of ~1 mA h cm^{-2}. The differences in transport properties and formation are likely more pronounced at higher mass loadings, as has been shown previously.[39] Fig. 5 shows comparable electrochemical performances after multiple cycles of testing. The printed NaAlg with octanol electrodes showcased the highest discharge capacity at 1C rate of approximately 120 mA h g^{-1}, along with a relatively stable long-term performance over 100 cycles (0% capacity fade). This discharge capacity was higher than that of the draw-down NaAlg with octanol electrodes, which exhibited a discharge capacity of approximately 112 mA h g^{-1} at 1C. Regarding the CMC/SBR electrodes without any octanol addition, they exhibited comparable cycling performances during the initial cycles. However, for the printed CMC/SBR electrodes, a decline in capacity was observed from the 80th cycle onwards. This

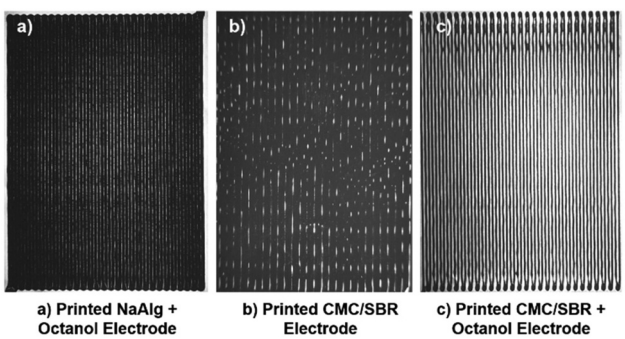

Fig. 2 Examples of printed electrodes in this work (a) sodium alginate (NaAlg) and octanol secondary solvent, (b) carboxy methyl cellulose (CMC) with styrene butene rubber (SBR) (c) carboxy methyl cellulose (CMC) with styrene butene rubber (SBR) and octanol secondary solvent.

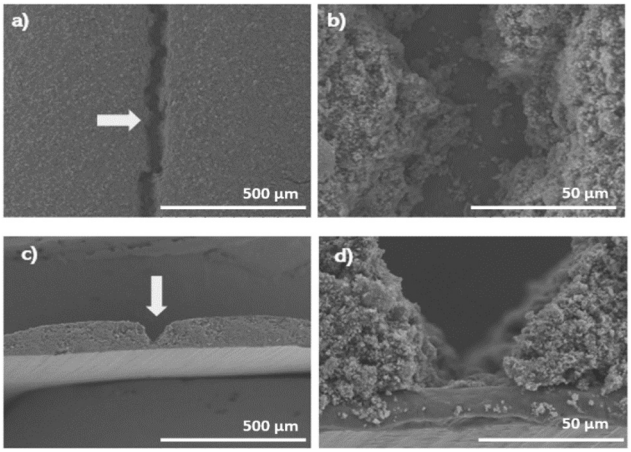

Fig. 3 SEM micrographs of the channels of LFP with alginate binder electrodes that were digitally printed, containing 0.5 wt% 1-octanol (a) top-view of the printed electrodes, revealing the existence of channels at a macro scale and (b) mesoscale. (c) Cross-sectional SEM micrograph of the printed electrodes at a macro scale and (d) mesoscale.

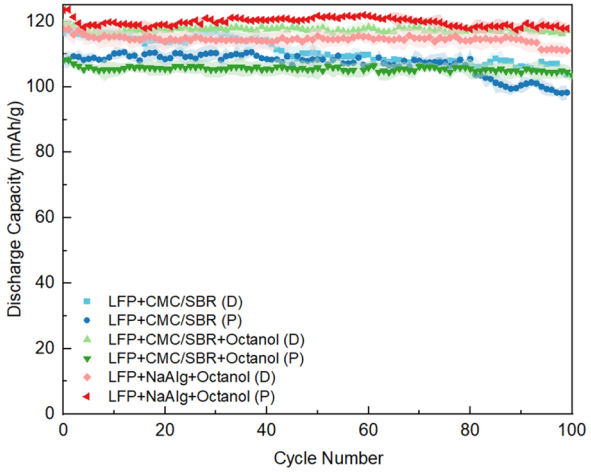

Fig. 5 The cycling performances of the samples involved in this project tested after 100 cycles. Here D is short for draw-down electrodes, P is short for printed electrodes; the shades of each plot indicate the error bars.

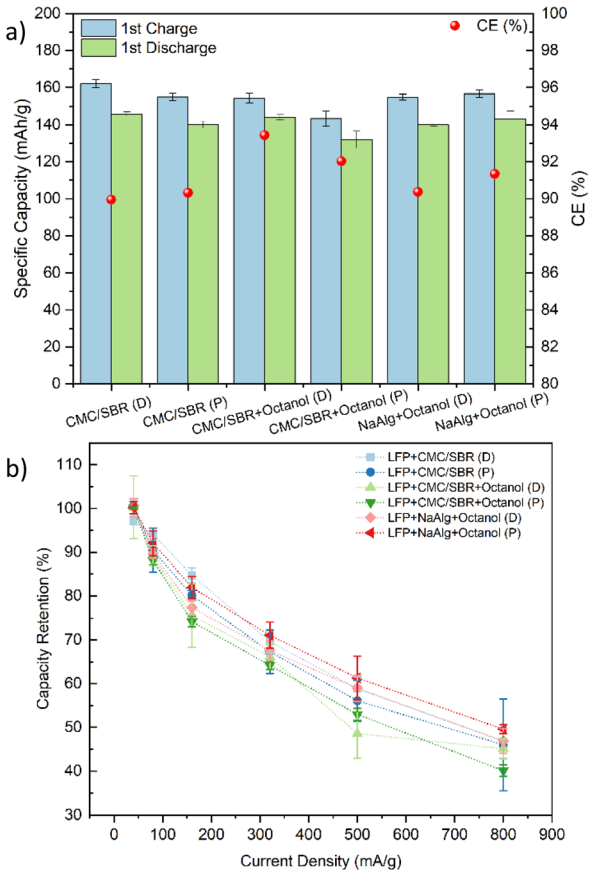

Fig. 4 (a) The capacity during formation tests and first cycle efficiencies of different electrodes (b) current density evaluations of the different electrode coatings. Here D is short for draw-down electrodes, P is short for printed electrodes.

decline in performance can be attributed to the CMC/SBR ink not being specifically designed for printing, resulting in an overall deterioration of the printed electrodes' performance. On the other hand, the CMC/SBR with octanol addition, intended to modify the ink rheology for printing, showed improvements in performance for the printed electrodes (discharge capacity of about 114 mA h g^{-1}) compared to the draw-down electrodes (discharge capacity of about 110 mA h g^{-1}). These results indicate that the printed LFP electrodes with alternative green binders exhibit electrochemical performances comparable to standard LFP cells using CMC/SBR binder materials *via* the casting method.

Another focus of this work was on the recovery rates and efficiencies for recovery of the materials from the electrodes during recycling processes. A flow chart which summarises the different electrode delamination accroaches trialled in this work is shown in Fig. S3.† The energy inputs were evaluated, and the recovery efficiency maximised for the lowest energy inputs. The most efficient process was a low power ultrasound delamination, which combined the delamination and binder negation process for the black mass recovery, and thus preserved the complexity of the LFP particles, for possible direct recycling. The delamination and separation efficiencies are noted for all the electrodes, as shown in Fig. 6, it is evident that both draw-down and printed CMC/SBR electrodes without octanol additions exhibited very low separation efficiency (~0%) within 10 minutes, even with an increased active material to solvent ratio. Additional ultrasonic treatment for 20 minutes did not yield satisfactory separation efficiencies (<10%) for these electrodes. Notably, for electrodes with similar mass loadings, the printed ones demonstrated higher separation efficiencies compared to draw-down electrodes when subjected to the same separation approaches. The superiority of printed NaAlg electrodes with octanol additions is particularly evident, achieving a separation efficiency of 85.81%

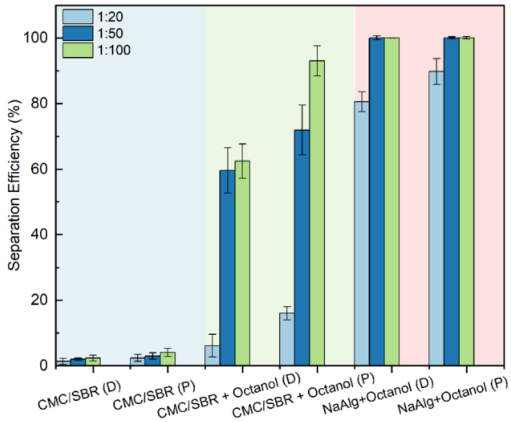

Fig. 6 Separation efficiencies of the samples involved in this project in an ultrasonic time of 10 minutes, with an active material to solvent (*i.e.* distilled water in this case) ratio of 1 : 20, 1 : 50 and 1 : 100 respectively. Here D is short for draw-down electrodes, P is short for printed electrodes.

within 10 minutes at an active material to solvent ratio of 1 : 20, surpassing the draw-down NaAlg electrodes with octanol additions (78.95%). Increased active material to solvent ratio contributed to enhanced separation efficiencies within the same time frame. As depicted in Fig. 6, most electrodes exhibited increased separation efficiencies after 10 minutes of low-power ultrasound treatment, as the active material to solvent ratio was raised from 1 : 20 to 1 : 100. This phenomenon is attributed to the mechanisms of ultrasonic bath mixing.[36,40] The presence of a larger quantity of water in the solvent leads to amplified convective motions induced by the ultrasound effect, aiding the dissolution of water-soluble binders. Additionally, ultrasonic waves in the solvent generate pressure and stretch cycles, leading to the formation of tiny bubbles with negative pressure. The cavitation effect causes these bubbles to burst,[41,42] generating significant impact forces that accelerate the delamination process. Further investigation is needed to optimize this liquid ratio, aiming to reduce solvent usage and wastage. Notably, in this study, the printed electrodes required less solvent while achieving higher separation efficiency, offering a promising avenue for improved sustainability and efficiency.

To investigate the disparities in separation efficiencies between printed and draw-down electrodes, the wettability of water droplets on different coatings and current collectors were examined. As can be observed from Fig. 7, the droplet was elongated upon the channels of the printed electrodes, whereas a normal droplet upon Al current collectors showed spherical appearance. The results revealed that all the printed electrodes exhibited lower contact angles compared to the draw-down coatings, indicating an improvement in wettability through the printing process.[43] Similarly, the printed CMC/SBR electrodes displayed reduced contact angles when compared to the draw-down CMC/SBR electrodes, although this improvement did not lead to a substantial difference in separation behaviours. However, the inclusion of octanol in the CMC/SBR coatings resulted in a significant increase in wettability, as evidenced by a remarkable rise in separation efficiency from 3% to 60%. This indicates that the addition of octanol played a crucial role in enhancing the wettability, thereby positively impacting the separation efficiency.

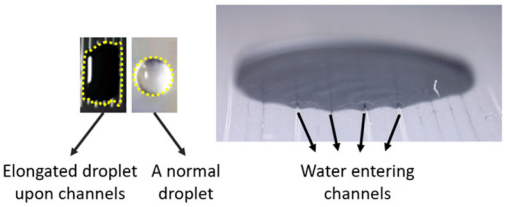

Fig. 7 Schematic illustration of the effect of channels on wettability of the coating materials under optical microscope, left: top view examination of elongated droplets upon channels and spherical droplets upon Al current collectors; right: cross-sectional view of printed LFP with NaAlg and octanol addition upon channels.

On the other hand, tortuosity is a measurement relating a curved or winding path compared to the direct ore straight line route. In batteries it is used to understand the ion transportation pathway in the electrolyte.[44] The cross-sectional SEM images of both draw-down and printed LFP electrodes were compared. The results are presented in Fig. 8, and as anticipated, a substantial decrease (34%) in tortuosity is observed for the printed electrodes. This is because in draw-down electrodes (Fig. 9a), the tortuosity value tends to be high due to the random distribution of the coating particles, resulting in indirect pathways for solvent transport. In contrast, the printed electrodes (Fig. 9b) exhibit channels that allow for direct transport of the solvent into the electrode. This characteristic is not only relevant for electrolyte mass transport,[45,46] but also plays a significant role in facilitating the imbibition of delamination solvents.

To compare the two electrode manufacturing processes data was compiled into the ERADE assessment matrix for com-

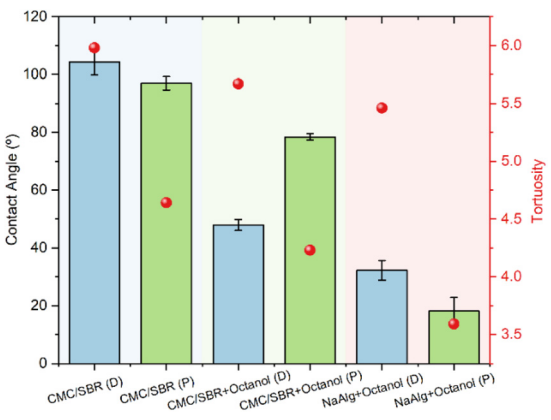

Fig. 8 Measured contact angle and tortuosity values for different electrodes. Here D is short for draw-down electrodes, P is short for printed electrodes.

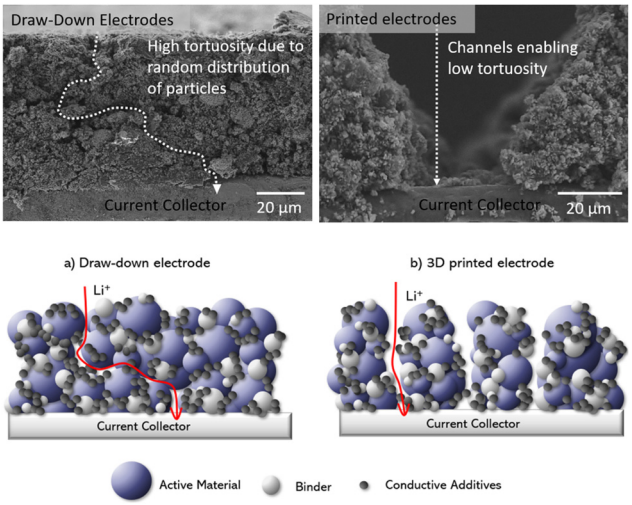

Fig. 9 Cross-sectional and schematic diagram showing the difference in Li^+ transportation paths (*i.e.* tortuosity) in draw-down and printed electrodes.

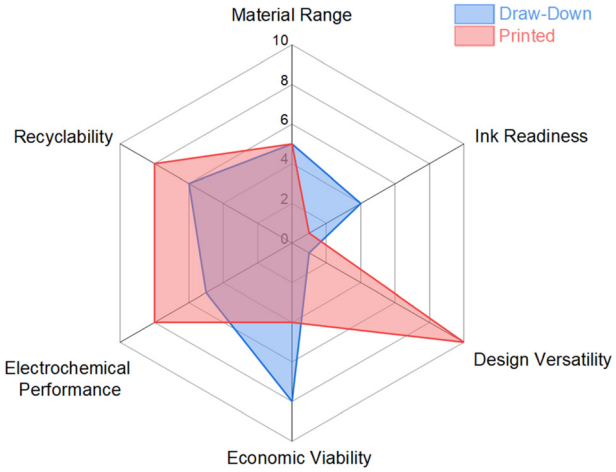

Fig. 10 Summary of ERADE assessment criteria, highlighting advantages and disadvantages of draw-down and 3D printed electrodes.

parative analysis (Table 1). As observed in Table 1, the printed electrodes, which utilise Na–alginate binders exhibited an overall higher score than their counterparts. A radar diagram summarizing the factors for both draw-down and printed electrodes is presented in Fig. 10. In general, while 3D printing techniques may incur higher costs during the initial stages, necessitating ink modification and equipment setup, they subsequently offer greater design flexibility, comparable electrochemical performances, and improved electrode separation with controlled disassembly and optimized recycling. This conclusion aligns with the findings of a study conducted by Lyu *et al.*,[35] which highlighted the advantages of designing 3D printed electrodes to enhance performance outcomes. The design of electrodes can significantly impact the manufacturing and recycling of lithium iron phosphate electrodes. Water-based binder systems offer cost-effective and environmentally friendly approaches for manufacturing electrodes through tape casting or printing methods. However, the traditional CMC-SBR system, while exhibiting good adhesive properties, has sustainability concerns as SBR is derived from oil and is not water-soluble. SBR adversely affects the wettability of the electrode in water, leading to low recovery efficiencies. To address this issue, the wettability can be enhanced by incorporating a small quantity of a secondary solvent, octanol, at

Table 1 Summary of the ERADE assessment matrix

		0–2 (inclusive)	3–5 (inclusive)	Draw-down electrodes	3D printed electrodes
Material range	Applicable to most types of materials?	No – certain types of materials are unavailable	Yes – applicable to most types of materials, *e.g.* metals, ceramics, *etc.*	5	5
Ink readiness	No requirement on further ink formulation (*e.g.* whether needs secondary fluid?)	No – requirement on ink formulation	Yes, or little requirement on ink formulation	4	1
Design versatility	Ability to produce patterns within electrode/construct complex electrode architecture?	No	Yes	0	5
	Ability to precisely deposit ink/ink controllability and electrode resolution?	No – little or no ink controllability, low resolution	Yes – excellent ink controllability, high resolution	1	5
Economic viability	Initial cost of Setup	More than £5000[34]	Less than £5000	5	2
	Energy consumption	More than 1 kW h[34]	Less than 1 kW h	3	2
Electrochemical performance	Specific capacity and rate compared to that of draw-down electrodes with CMC/SBR	Capacity and rate not as good as CMC/SBR	Capacity and rate are similar or improved compared to CMC/SBR	3	3
	Tortuosity	>1	Able to reach a tortuosity of 1	2	5
Recyclability (Separation)	Separation efficiency *via* water immersion	<90% within 5 min (Na–Alg binder system)	≥90% within 5 min (Na–Alg binder system)	2	4
	Recovery rate of active material	<90%	≥90%	4	4
Total				30	38

the ink level. Octanol not only improves the final electrode's wettability but also modifies the fluid characteristics to facilitate successful printing and shape retention during the printing process. Consequently, the printed electrodes demonstrate improved wettability, as evidenced by lower contact angles, and possess lower tortuosity pathways for solvent imbibition. This combined effect leads to significantly improved recovery rates of the $LiFePO_4$ electrode during recycling. Overall, the study highlights that both wettability and tortuosity are crucial considerations in electrode design to achieve better recovery rates and enhance the sustainability and recycling efficiency of energy storage systems.

In this work we are **preventing waste** in two manners, the first is by reducing the waste which occurs during the manufacturing processes, and the second is by maximising the recovery of the materials. Typical ways to produce electrodes such as slot-die coatings produce double sided coating, which are then punched to make the electrodes to size.[47] In this work electrodes of exactly the right size can be printed, thus removing the need for cleaning of the tabs, and waste electrode. In addition, the electrodes are **designed for separation**, both the water-based binders, but also the microstructural design mean that the **efficiency** and recovery of the active material, $LiFePO_4$ and the aluminium current collector is **maximised**. The water-based binders, such as alginate, carboxy methyl cellulose and octanol biodegrade rapidly in aquatic environments. Since the binders and octanol are bio-degradable and the recovery of the electrode materials are maximised for recovery, the resulting water after separation will break down to innocuous degradation products such as water and CO_2, which will not persist in the environment, therefore **designing for degradation**. '**Inherent rather than circumstantial**', the electrode process manufacturing and recycling process has been designed to ensure that the materials and energy inputs and outputs are as non-hazardous as possible.

Conclusions

In this work, the ability to design electrodes for improved recovery rates of lithium iron phosphate has been investigated. Two water-based renewable bio-degradable binder systems, sodium alginate (NaAlg) and carboxy-methyl cellulose (CMC) the latter with styrene butene rubber (SBR) for flexibility, have been used for producing coatings using tape-cast and direct ink printing methods. The electrodes were printed at areal capacities of 1 mA h cm^{-2} for comparison, and both binder systems produced electrodes which exhibited comparable electrochemical results. To ensure successful direct ink writing, the printed electrode inks required rheological modification to prevent slumping, achieved by adding 0.5 wt% octanol, also biodegradable, as an additive to form an extrudable paste. The printed electrodes exhibited lower tortuosity due to the presence of channels in the coating. Across all cases, the printed electrodes demonstrated improved wettability, as confirmed by contact angle measurements. After a 10-minute delamination in a low power ultrasound bath, a higher separation efficiency was observed for printed alginate electrodes (86%) compared to draw-down electrodes (79%). For the CMC-SBR systems, the samples containing octanol showed a recovery improvement of more than 72% in the printed sample compared to only 3% recovery in the absence of octanol. The improved wettability and lower tortuosity facilitated the soaking of solvents into the electrode structure which helps to remove the water-soluble binders and hence improve recovery rates of $LiFePO_4$. An assessment matrix for qualitatively evaluating the design, ERADE, is proposed, giving a score of 30 for draw-down techniques and 38 for 3D printing, suggesting that overall 3D printed electrodes are favourable from perspectives of designing electrode format for disassembly and recycling.

In conclusion, this study emphasizes the critical role of electrode design in the recycling of LIBs and lays the groundwork for future research into novel design principles for printed electrodes. Such designs have the potential to offer improved recycling properties without compromising electrochemical performance. This aspect is particularly relevant for low-value materials like $LiFePO_4$ or sodium-ion materials, where achieving economic materials recovery poses challenges. Overall, this study highlights the importance of considering electrode design in sustainable battery technologies.

Author contributions

Conceptualization, GD, EK.; methodology, GD, EK, LY.; formal analysis, GD, LY.; investigation, GD, LY; writing – original draft preparation, LY, GD.; writing – review and editing, LY, GD, EK; visualization, LY.; supervision, GD, EK.; project administration, EK.; funding acquisition, EK. All authors have read and agreed to the published version of the manuscript.

Conflicts of interest

There are no conflicts to declare.

Acknowledgements

The authors wish to thank the Energy Materials Group at University of Birmingham for their help and support during the project. Especially, the authors would like to thank Brij Kishore and Dave Burnett for their help on jet milling. The authors would also like to acknowledge the support of the Faraday Institution funded project ReLiB project (Grant Codes FIRG005, FIRG027 and FIRG057) and the UKRI Interdisciplinary Circular Economy Centre for Technology Metals (TechMet) Grant No. EP/V011855/1 for funding.

References

1 G. D. J. Harper, E. Kendrick, P. A. Anderson, W. Mrozik, P. Christensen, S. Lambert, *et al.*, Roadmap for a sustainable circular economy in lithium-ion and future battery technologies, *JPhys Energy*, 2023, **5**, 021501, DOI: **10.1088/2515-7655/acaa57**.

2 S. Jenkins, *State of Battery Recycling – Can We Meet Our LIB Recycling Obligations by 2030?* **https://caper-usa.com/news/state-of-battery-recycling-can-we-meet-our-lib-recycling-obligations-by-2030/** (accessed September 14, 2022).

3 R. Sommerville, J. Shaw-Stewart, V. Goodship, N. Rowson and E. Kendrick, A review of physical processes used in the safe recycling of lithium ion batteries, *Sustainable Mater. Technol.*, 2020, **25**, e00197, DOI: **10.1016/j.susmat.2020.e00197**.

4 R. Sommerville, P. Zhu, M. A. Rajaeifar, O. Heidrich, V. Goodship and E. Kendrick, A qualitative assessment of lithium ion battery recycling processes, *Resour., Conserv. Recycl.*, 2021, **165**, 105219, DOI: **10.1016/j.resconrec.2020.105219**.

5 D. Gastol, J. Marshall, E. Cooper, C. Mitchell, D. Burnett, T. Song, *et al.*, Reclaimed and Up-Cycled Cathodes for Lithium-Ion Batteries, *Glob. Chall.*, 2022, **6**, 2200046, DOI: **10.1002/gch2.202200046**.

6 D. L. Thompson, J. M. Hartley, S. M. Lambert, M. Shiref, G. D. J. Harper, E. Kendrick, *et al.*, The importance of design in lithium ion battery recycling-a critical review, *Green Chem.*, 2020, **22**, 7585–7603, DOI: **10.1039/d0gc02745f**.

7 S. Scott, Z. Islam, J. Allen, T. Yingnakorn, A. Alflakian, J. Hathaway, *et al.*, Designing lithium-ion batteries for recycle: The role of adhesives, *Energy*, 2023, **1**, 100023, DOI: **10.1016/j.nxener.2023.100023**.

8 D. L. Wood, J. Li and C. Daniel, Prospects for reducing the processing cost of lithium ion batteries, *J. Power Sources*, 2015, **275**, 234–242, DOI: **10.1016/J.JPOWSOUR.2014.11.019**.

9 Per- and polyfluoroalkyl substances (PFAS) – ECHA n.d. **https://echa.europa.eu/hot-topics/perfluoroalkyl-chemicals-pfas** (accessed August 11, 2023).

10 N. D. Tyrrell, A Proposal That Would Ban Manufacture, Supply, and Use of All Fluoropolymers and Most Fluorinated Reagents within the Entire EU, *Org. Process Res. Dev.*, 2023, **27**(8), 1422–1426, DOI: **10.1021/acs.oprd.3c00199**.

11 R. Schmuch, R. Wagner, G. Hörpel, T. Placke and M. Winter, Performance and cost of materials for lithium-based rechargeable automotive batteries, *Nature Energy*, 2018, **3**, 267, DOI: **10.1038/S41560-018-0107-2**.

12 B. Améduri and H. Hori, Recycling and the end of life assessment of fluoropolymers: recent developments, challenges and future trends, *Chem. Soc. Rev.*, 2023, **52**, 4208–4247, DOI: **10.1039/D2CS00763K**.

13 H. Cai, Y. Wang, M. Xu, L. Cheng, Z. Liu, Z. Li, *et al.*, Low cost, green and effective preparation of multifunctional flexible silk fabric electrode with ultra-high capacitance retention, *Carbon*, 2022, **188**, 197–208, DOI: **10.1016/j.carbon.2021.11.042**.

14 L. Xu, H. Sitinamaluwa, H. Li, J. Qiu, Y. Wang, C. Yan, *et al.*, Low cost and green preparation process for α-Fe2O3@gum arabic electrode for high performance sodium ion batteries, *J. Mater. Chem. A*, 2017, **5**, 2102–2109, DOI: **10.1039/C6TA08918F**.

15 R. McNair, G. Szekely and R. A. W. Dryfe, Sustainable processing of electrodes for membrane capacitive deionization (MCDI), *J. Cleaner Prod.*, 2022, **342**, 130922, DOI: **10.1016/j.jclepro.2022.130922**.

16 Z. P. Cai, Y. Liang, W. S. Li, L. D. Xing and Y. H. Liao, Preparation and performances of LiFePO4 cathode in aqueous solvent with polyacrylic acid as a binder, *J. Power Sources*, 2009, **189**, 547–551, DOI: **10.1016/J.JPOWSOUR.2008.10.040**.

17 I. Doberdò, N. Löffler, N. Laszczynski, D. Cericola, N. Penazzi, S. Bodoardo, *et al.*, Enabling aqueous binders for lithium battery cathodes – Carbon coating of aluminum current collector, *J. Power Sources*, 2014, **248**, 1000–1006, DOI: **10.1016/J.JPOWSOUR.2013.10.039**.

18 F. Zou, A. Manthiram, F. Zou and A. Manthiram, A Review of the Design of Advanced Binders for High-Performance Batteries, *Adv. Energy Mater.*, 2020, **10**, 2002508, DOI: **10.1002/AENM.202002508**.

19 A. F. Léonard and N. Job, Safe and green Li-ion batteries based on LiFePO4 and Li4Ti5O12 sprayed as aqueous slurries with xanthan gum as common binder, *Mater. Today Energy*, 2019, **12**, 168–178, DOI: **10.1016/J.MTENER.2019.01.008**.

20 S. Scott, J. Terreblanche, D. L. Thompson, C. Lei, J. M. Hartley, A. P. Abbott, *et al.*, Gelatin and Alginate Binders for Simplified Battery Recycling, *J. Phys. Chem. C*, 2022, **126**, 8489–8498, DOI: **10.1021/acs.jpcc.2c01282**.

21 J. He, H. Zhong, J. Wang and L. Zhang, Investigation on xanthan gum as novel water soluble binder for LiFePO4 cathode in lithium-ion batteries, *J. Alloys Compd.*, 2017, **714**, 409–418, DOI: **10.1016/j.jallcom.2017.04.238**.

22 J. Liu, H. Yuan, X. Tao, Y. Liang, S. J. Yang, J.-Q. Huang, *et al.*, Recent progress on biomass-derived ecomaterials toward advanced rechargeable lithium batteries, *EcoMat*, 2020, **2**, e12019, DOI: **10.1002/eom2.12019**.

23 Y. Ren, Z. Liu, F. Pourpoint, A. R. Armstrong, C. P. Grey and P. G. Bruce, Nanoparticulate TiO2(B): An Anode for Lithium-Ion Batteries, *Angew. Chem., Int. Ed.*, 2012, **51**, 2164–2167, DOI: **10.1002/ANIE.201108300**.

24 H. Hu, L. Yu, X. Gao, Z. Lin and X. W. Lou, Hierarchical tubular structures constructed from ultrathin TiO2(B) nanosheets for highly reversible lithium storage, *Energy Environ. Sci.*, 2015, **8**, 1480–1483, DOI: **10.1039/C5EE00101C**.

25 X. Zhu, X. Yang, C. Lv, S. Guo, J. Li, Z. Zheng, *et al.*, New Approach to Create TiO2(B)/Carbon Core/Shell Nanotubes: Ideal Structure for Enhanced Lithium Ion Storage, *ACS Appl. Mater. Interfaces*, 2016, **8**, 18815–18821, DOI: **10.1021/ACSAMI.6B04588/SUPPL_FILE/AM6B04588_SI_001.PDF**.

26 C. D. Reynolds, S. D. Hare, P. R. Slater, M. J. H. Simmons and E. Kendrick, Rheology and Structure of Lithium-Ion Battery Electrode Slurries, *Energy Technol.*, 2022, **10**, 2200545, DOI: 10.1002/ente.202200545.

27 S. H. Lee, C. Huang, C. Johnston and P. S. Grant, Spray printing and optimization of anodes and cathodes for high performance Li-Ion batteries, *Electrochim. Acta*, 2018, **292**, 546–557, DOI: 10.1016/j.electacta.2018.09.132.

28 D. Gastol, M. Capener, C. Reynolds, C. Constable and E. Kendrick, Microstructural design of printed graphite electrodes for lithium-ion batteries, *Mater. Des.*, 2021, **205**, 109720, DOI: 10.1016/J.MATDES.2021.109720.

29 J. Wang, Q. Sun, X. Gao, C. Wang, W. Li, F. B. Holness, *et al.*, Toward High Areal Energy and Power Density Electrode for Li-Ion Batteries via Optimized 3D Printing Approach, *ACS Appl. Mater. Interfaces*, 2018, **10**, 39794–39801, DOI: 10.1021/ACSAMI.8B14797/SUPPL_FILE/AM8B14797_SI_001.PDF.

30 A. Gören, J. Mendes, H. M. Rodrigues, R. E. Sousa, J. Oliveira, L. Hilliou, *et al.*, High performance screen-printed electrodes prepared by a green solvent approach for lithium-ion batteries, *J. Power Sources*, 2016, **334**, 65–77, DOI: 10.1016/j.jpowsour.2016.10.019.

31 F. Zhang, K. Wu, X. Xu, W. Wu, X. Hu, K. Yu, *et al.*, 3D Printing of Graphite Electrode for Lithium-Ion Battery with High Areal Capacity, *Energy Technol.*, 2021, **9**, 2100628, DOI: 10.1002/ente.202100628.

32 G. Boothroyd and L. Alting, Design for Assembly and Disassembly, *CIRP Ann.*, 1992, **41**, 625–636, DOI: 10.1016/S0007-8506(07)63249-1.

33 K. Zaghib, M. Dontigny, A. Guerfi, P. Charest, I. Rodrigues, A. Mauger, *et al.*, Safe and fast-charging Li-ion battery with long shelf life for power applications, *J. Power Sources*, 2011, **196**, 3949–3954, DOI: 10.1016/J.JPOWSOUR.2010.11.093.

34 G. Zubi, R. Dufo-López, M. Carvalho and G. Pasaoglu, The lithium-ion battery: State of the art and future perspectives, *Renewable Sustainable Energy Rev.*, 2018, **89**, 292–308, DOI: 10.1016/j.rser.2018.03.002.

35 Z. Lyu, G. J. H. Lim, R. Guo, Z. Pan, X. Zhang, H. Zhang, Z. He, W. Chen, J. Ding and J. Wang, 3D-printed electrodes for lithium metal batteries with high areal capacity and high-rate capability, *Energy Storage Materials*, 2020, 366–342, DOI: 10.1016/j.ensm.2019.07.041.

36 L. P. He, S. Y. Sun, X. F. Song and J. G. Yu, Recovery of cathode materials and Al from spent lithium-ion batteries by ultrasonic cleaning, *Waste Manage.*, 2015, **46**, 523–528, DOI: 10.1016/j.wasman.2015.08.035.

37 S. J. Cooper, A. Bertei, P. R. Shearing, J. A. Kilner and N. P. Brandon, TauFactor: An open-source application for calculating tortuosity factors from tomographic data, *SoftwareX*, 2016, **5**, 203–210, DOI: 10.1016/J.SOFTX.2016.09.002.

38 M. Bercea, Rheology as a Tool for Fine-Tuning the Properties of Printable Bioinspired Gels, *Molecules*, 2023, **28**, 2766, DOI: 10.3390/molecules28062766.

39 L. Li, H. Tan, X. Yuan, H. Ma, Z. Ma, Y. Zhao, *et al.*, Direct ink writing preparation of LiFePO4/MWCNTs electrodes with high-areal Li-ion capacity, *Ceram. Int.*, 2021, **47**, 21161–21166, DOI: 10.1016/j.ceramint.2021.04.119.

40 M. Jafari, M. M. Torabian and A. Bazargan, A Facile Chemical-Free Cathode Powder Separation Method for Lithium Ion Battery Resource Recovery, *J. Energy Storage*, 2020, **31**, 101564, DOI: 10.1016/j.est.2020.101564.

41 L. Azar, Cavitation in ultrasonic cleaning and cell disruption, *Control. Environ.*, 2009, 14–17.

42 N. A. Oz and C. C. Yarimtepe, Ultrasound assisted biogas production from landfill leachate, *Waste Manage.*, 2014, **34**, 1165–1170, DOI: 10.1016/j.wasman.2014.03.003.

43 L. H. Lee, Roles of molecular interactions in adhesion, adsorption, contact angle and wettability, *J. Adhes.*, 2012, **7**, 583–634, DOI: 10.1163/156856193X00871.

44 A. Wang, S. O'Kane, F. B. Planella, J. L. Houx, K. O'Regan, M. Zyskin, *et al.*, Review of parameterisation and a novel database (LiionDB) for continuum Li-ion battery models, *Prog. Energy*, 2022, **4**, 032004, DOI: 10.1088/2516-1083/AC692C.

45 R. Rodriguez, L. J. Deiner, H. Tsao and J. P. Fellner. Aerosol Jet-Printed LFP Cathodes with Bimodal Pore Distribution Improve the Rate Capability of LIB Cells 2021. DOI: 10.1021/acsaem.1c01678.

46 J. Wu, Z. Ju, X. Zhang, C. Quilty, K. J. Takeuchi, D. C. Bock, *et al.*, Ultrahigh-Capacity and Scalable Architected Battery Electrodes via Tortuosity Modulation, *ACS Nano*, 2021, **15**, 19109–19118, DOI: 10.1021/ACSNANO.1C06491/SUPPL_FILE/NN1C06491_SI_001.PDF.

47 C. D. Reynolds, P. R. Slater, S. D. Hare, M. J. H. Simmons and E. Kendrick, A review of metrology in lithium-ion electrode coating processes, *Mater. Des.*, 2021, **209**, 109971, DOI: 10.1016/J.MATDES.2021.109971.